(1994)] showed a large-scale anticyclonic gyre in the general vicinity of the gyre shown in Fig. 1C. However, Reid's gyre and the one depicted in Fig. 1C have substantial differences in their vertical structure and horizontal substructure.
7. Southward flow of North Atlantic Deep Water on the eastern side of the Mid-Atlantic Ridge is supported by P. M. Saunders [*J. Mar. Res.* **40**, 641 (1982)], S. Gana and C. Provost [*J. Mar. Syst.* **4**, 67 (1993)], and J. Paillet and H. Mercier (*Deep-Sea Res., Part I*, in press).
8. Topographic sill depths of ~1000 m are a barrier for flow of this density into the Nordic Seas.
9. L. V. Worthington, *Johns Hopkins Oceanogr. Stud.* **6**, (1976); R. A. Clarke, H. W. Hill, R. F. Reininger, B. A. Warren, *J. Phys. Oceanogr.* **10**, 25 (1980); M. S. McCartney, *Prog. Oceanogr.* **29**, 283 (1992); W. J. Schmitz and M. S. McCartney, *Rev. Geophys.* **31**, 29 (1993).
10. R. S. Pickart and W. M. Smethie, *J. Phys. Oceanogr.* **23**, 2602 (1993).
11. J. Paillet, M. Arhan, M. S. McCartney, in preparation.
12. P. B. Rhines and W. R. Holland, *Dyn. Atmos. Oceans* **3**, 289 (1979).
13. W. R. Holland, *Geophys. Fluid Dyn.* **4**, 187 (1973).
14. R. Gerdes and C. Köberle, *J. Phys. Oceanogr.* **25**, 2624 (1995).
15. These gyres at intermediate depths are distinct from the smaller scale gyres at abyssal depths that are more clearly associated with the basin topography.
16. P. B. Rhines and W. R. Young, *J. Fluid Mech.* **122**, 347 (1982).
17. W. R. Holland and P. B. Rhines, *J. Phys. Oceanogr.* **10**, 1010 (1980).
18. S. McDowell, P. Rhines, T. Keffer, *ibid*. **12**, 1417 (1982); T. Keffer, *ibid*. **15**, 509 (1985); J. L. Sarmiento, C. G. H. Rooth, W. Roether, *J. Geophys. Res.* **87**, 8047 (1982).
19. J. Pedlosky, *Ocean Circulation Theory* (Springer-Verlag, New York, 1996).
20. Potential vorticity is calculated as $f^{1}/\sigma_{o} \times \partial\sigma_{n}/\partial z$, where f is the planetary vorticity, z is the vertical coordinate, and σ_{o} is a constant potential density. The vertical derivative is computed locally over a nominal depth of 100 m. In an effort to approximate neutral surfaces [T. J. McDougall, *J. Phys. Oceanogr.* **17**, 1950 (1987)], potential vorticity was also calculated as f/h, where h is the distance between two locally referenced isopycnals. The differences in the two methods were insignificant to the results of this study; that is, the region and extent of homogenization were the same with either calculation.
21. M. S. McCartney and L. D. Talley, *ibid*. **12**, 1169 (1982).
22. J. O'Dwyer and R. G. Williams (*J. Phys. Oceanogr.*, in press) report, from an analysis of the Levitus data set, possible regions of homogenization at abyssal depths in the western North Atlantic.
23. An absolute flow field was calculated for $\sigma_{2} = 36.95$ by differentiation of a modified [H.-M. Zhang and N. G. Hogg, *J. Mar. Res.* **50**, 385 (1992)] Montgomery stream-function field [R. B. Montgomery, *Bull. Am. Meteorol. Soc.* **18**, 210 (1937)] with $\sigma_{3} = 41.45$ (at ~3000 m) as the level of no motion.
24. D. L. Musgrave, *J. Geophys. Res.* **90**, 7037 (1985).
25. Surfaces shallower than $\sigma_{2} = 36.95$ show counter-rotating gyres separated by this instability region in the western North Atlantic, which suggests the importance of eddy flux divergence in the forcing of the gyres.
26. J. Pedlosky, *J. Phys. Oceanogr.* **13**, 2121 (1983).
27. N. Hogg, *Deep-Sea Res. Part A* **30**, 945 (1983).
28. P. B. Rhines and W. R. Young, *J. Mar. Res.* **40**, 559 (1982).
29. P. Cessi, G. Ierley, W. Young, *J. Phys. Oceanogr.* **17**, 1640 (1987); P. Cessi, *ibid*. **18**, 662 (1988).
30. W. J. Jenkins and P. B. Rhines, *Nature* **286**, 877 (1980); R. S. Pickart, *Deep-Sea Res. Part A* **39**, 1553 (1992); W. M. Smethie, *Prog. Oceanogr.* **31**, 51 (1993).
31. I thank J. Pedlosky for his aid in the interpretation of these fields and P. Rhines for his comments on the manuscript. Support from NSF (grant OCE- 9629489) is gratefully acknowledged.

20 February 1997; accepted 22 May 1997

Maximum and Minimum Temperature Trends for the Globe

David R. Easterling,* Briony Horton, Philip D. Jones, Thomas C. Peterson, Thomas R. Karl, David E. Parker, M. James Salinger, Vyacheslav Razuvayev, Neil Plummer, Paul Jamason, Christopher K. Folland

Analysis of the global mean surface air temperature has shown that its increase is due, at least in part, to differential changes in daily maximum and minimum temperatures, resulting in a narrowing of the diurnal temperature range (DTR). The analysis, using station metadata and improved areal coverage for much of the Southern Hemisphere landmass, indicates that the DTR is continuing to decrease in most parts of the world, that urban effects on globally and hemispherically averaged time series are negligible, and that circulation variations in parts of the Northern Hemisphere appear to be related to the DTR. Atmospheric aerosol loading in the Southern Hemisphere is much less than that in the Northern Hemisphere, suggesting that there are likely a number of factors, such as increases in cloudiness, contributing to the decreases in DTR.

The global mean surface air temperature has risen about 0.5°C during the 20th century (*1*). Analysis has shown that this rise has resulted, in part, from the daily minimum temperature increasing at a faster rate or decreasing at a slower rate than the daily maximum, resulting in a decrease in the DTR for many parts of the world (*2, 3*). Decreases in the DTR were first identified in the United States, where large-area trends show that maximum temperatures have remained constant or have increased only slightly, whereas minimum temperatures have increased at a faster rate (*4*). Similar changes have been found for other parts of the world as data have become available, allowing more global analyses (*2, 3*). However, in some areas the pattern has been different: In parts of New Zealand (*5*) and alpine regions of central Europe (*6*), maximum and minimum temperature have increased at similar rates, and in India, the DTR has increased as a result of a decrease in the minimum temperature (*7*). To evaluate these varying results, we conducted an expanded analysis on global and regional scales.

Local effects such as urban growth, irrigation, desertification, and variations in local land use can all affect the DTR (*3*); in particular, urbanized areas often show a narrower DTR than nearby rural areas (*8*). Large-scale climatic effects on the DTR include increases in cloud cover, surface evaporative cooling from precipitation, greenhouse gases, and tropospheric aerosols (*9, 10*). Recent studies have demonstrated a strong relation between trends of the DTR and decreases in pan evaporation over the former Soviet Union and the United States (*11*), suggesting that the DTR decrease in these areas is influenced by increases of cloud amount and reduced insolation (*1*). Furthermore, recent modeling studies have suggested that the decrease in the DTR may be a result of a combination of direct absorption of infrared portions of incoming solar radiation, aerosols, and water-vapor feedbacks, including surface evaporative effects (*12*).

We analyzed monthly averaged maximum and minimum temperatures and the DTR at 5400 observing stations around the world. Each time series from each station was subjected independently to homogeneity analyses and adjustments according to recently developed techniques (*13*). In general, these homogeneity adjustments have little effect on large-area averages (global or hemispheric), but they can have a noticeable effect on smaller regions (*14*), particularly when comparing trends at individual or adjacent grid boxes.

Our data covers 54% of the total global land area, 17% more than in previous studies (*3*). Most of the increases are in the Southern Hemisphere, with the addition of data for South America, New Zealand, all of Australia, a number of Pacific islands, and Indonesia. Data were also in-

D. R. Easterling, T. C. Peterson, T. R. Karl, National Climatic Data Center, Asheville, NC 28801, USA.
B. Horton, D. E. Parker, C. K. Folland, Hadley Center, Meteorological Office, Bracknell, Berkshire, UK.
P. D. Jones, Climatic Research Unit, University of East Anglia, Norwich, UK.
M. J. Salinger, National Institute of Water and Atmospheric Research, Auckland, New Zealand.
V. Razuvayev, All-Russia Research Institute of Hydrometeorological Information, Obninsk, Russia.
N. Plummer, National Climate Center, Bureau of Meteorology, Melbourne, Australia.
P. Jamason, DynTel Inc., National Climatic Data Center, Asheville, NC 28801, USA.

*To whom correspondence should be addressed: E-mail: deasterl@ncdc.noaa.gov

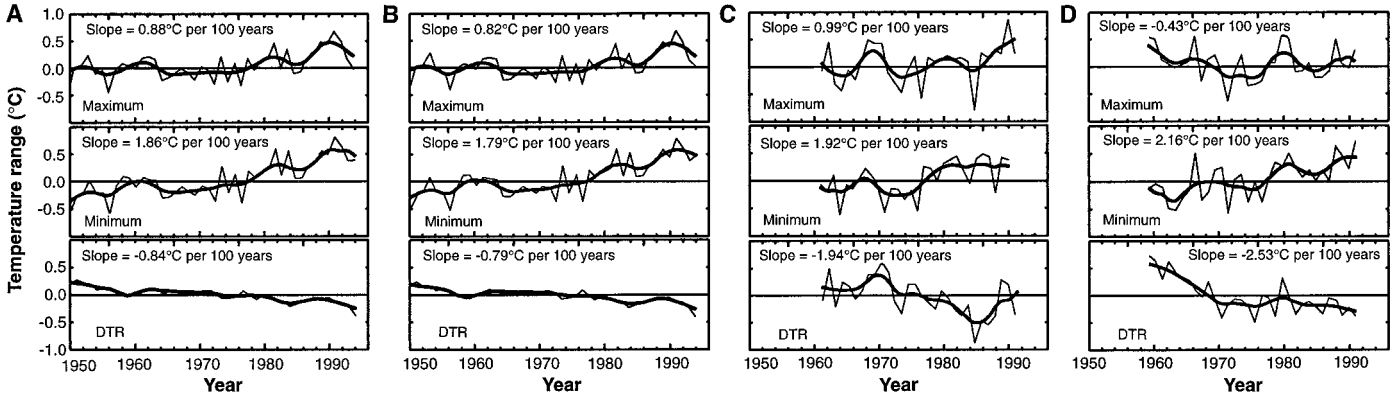

Fig. 1. Time series of annual average maximum temperature, minimum temperature, and DTR for (**A**) the globe, using all available stations, (**B**) the globe, using only nonurban stations, (**C**) Chile and Argentina, using only nonurban stations, and (**D**) Southeast Asia, using only nonurban stations. The heavy line is the result of smoothing with a nine-point binomial filter with reflected ends. Trends (slopes) for the maximum temperatures in (C) and (D) are not statistically significant at the 0.05 level (two-tailed *t* test).

cluded for tropical and subtropical areas, such as the Caribbean, parts of Africa, Iran, Pakistan, and Southeast Asia. However, there are still large parts of the world that remain unanalyzed because of a lack of data, particularly in the tropics, and updating these data remains a problem, as shown by our analysis ending in 1993 (*15*).

In our analysis, we first calculated anomalies from the mean of the base period of 1961 to 1985 for all stations in each 5° by 5° latitude-longitude grid box. The global or hemispheric value for each year was then determined by area-weighting each grid box and averaging all the weighted grid-box values. The overall global trend for the maximum temperature is +0.88°C per 100 years, which is consistent with an earlier finding (*3*). However, the trend for the minimum temperature is +1.86°C per 100 years, which is considerably less than that found in previous analyses. This reduction in the trend for minimum temperature results in a smaller trend in the DTR of −0.84°C per 100 years. This finding is not surprising, because most of the data added here are for tropical and subtropical regions, where temperature changes are not expected to be as large as in regions of higher latitude (*1*), and because of the effects of the Mount Pinatubo eruption. The temperature increases for these 25 years are greater than those over the rest of the 20th century, reflecting the stronger warming during the latter half of this century (*1*).

We examined urban effects on global and hemispheric trends using a metadata set developed at the U.S. National Climatic Data Center. These data indicate whether a station is in an urban or nonurban environment, where urban is defined as a city of 50,000 or greater population (*16*). Approximately 1300 of the original 5400 stations were determined to be urban by this rough measure. The globally averaged time series for the annual maximum and minimum temperature and DTR calculated using only nonurban stations show only slight differences from those calculated using all available stations (Fig. 1). The trend for the maximum temperature excluding the effects of large urban areas is +0.82°C per 100 years, and for the minimum temperature is +1.79°C per 100 years; the DTR trend is −0.79°C per 100 years. The difference in the trends for the maximum and minimum temperatures is about 0.1°C per 100 years, which is consistent with other estimated urban effects on global mean temperature time series (*16*, *17*). The likely effects of the Mount Pinatubo eruption are seen in both the maximum and minimum temperature time series, which show a distinct drop in 1992. The maximum temperature continued to drop in 1993, whereas the minimum stabilized, which resulted in a continued decrease in the DTR.

Maximum temperatures have increased over most areas with the notable exception of eastern Canada, the southern United States, portions of eastern Europe, southern China, and parts of southern South America (Fig. 2). The minimum temperatures, however, increased almost everywhere except eastern Canada and small areas of eastern Europe and the Middle East. The DTR decreased in most areas, except over middle Canada and parts of southern Africa, southwest Asia, Eu-

Table 1. Annual and seasonal trends from 1950 to 1993 for maximum temperature, minimum temperature, and DTR for the globe and the Northern and Southern hemispheres. Trends calculated using only nonurban stations are given, with the trends using all stations given in parentheses.

Season	Trend (°C per 100 years)		
	Maximum temp.	Minimum temp.	DTR
	Global		
D-J-F	1.10 (1.31)	2.48 (2.76)	−1.35 (−1.37)
M-A-M	1.25 (1.17)	2.26 (2.27)	−1.04 (−1.09)
J-J-A	0.47 (0.40*)	1.13 (1.12)	−0.65 (−0.69)
S-O-N	0.05* (−0.01*)	0.94 (0.98)	−0.89 (−0.92)
	Northern Hemisphere		
D-J-F	1.26 (1.52)	2.74 (3.04)	−1.44 (−1.48)
M-A-M	1.39 (1.29)	2.28 (2.30)	−0.90 (−1.01)
J-J-A	0.25* (0.25*)	1.05 (1.04)	−0.79 (−0.77)
S-O-N	−0.12* (−0.01*)	0.72* (0.83)	−0.84 (−0.90)
Annual	0.77 (0.87)	1.74 (1.84)	−0.89 (−0.89)
	Southern Hemisphere		
D-J-F	0.66 (0.62)	1.61 (1.66)	−1.00 (−0.93)
M-A-M	0.59* (0.55*)	1.98 (1.97)	−1.37 (−1.31)
J-J-A	1.27 (1.18)	1.41 (1.40)	−0.08* (−0.12*)
S-O-N	0.69* (0.84)	1.74 (1.69)	−1.08 (−1.02)
Annual	0.91 (0.84)	1.81 (1.80)	−0.59 (−0.60)

*Not significant at the 0.05 level (two-tailed *t* test).

rope, interior Australia, and the western tropical Pacific islands. It should be kept in mind that each grid-box value is the average of 1 to 20 or more stations within that grid box, and that the value for any one grid box is subject to any problems inherent in the station data. Because the DTR is the maximum temperature minus the minimum temperature, the DTR can decrease when the trend in the maximum or minimum temperature is down, up, or unchanging. This relation contributes to the appearance of less spatial coherence on the DTR map than on the other two. Seasonally, the strongest changes in the DTR were in the boreal winter season, and the smallest changes were during the boreal summer (Table 1), suggesting that there is an element of a seasonal cycle in the changes.

Maximum temperatures in southern South America and in Southeast Asia (Fig. 1), two areas not previously analyzed, did not change significantly, although the data for Southeast Asia suggest that temperatures there decreased slightly. In both regions, minimum temperatures increased significantly, resulting in a significant decrease in DTR. Furthermore, minimum temperatures in the Southern Hemisphere increased, and because the tropospheric aerosol load in this hemisphere is much less than that in the Northern Hemisphere, additional factors, such as increases in cloudiness (*9*), are likely contributing to observed increases in nighttime temperature. The minimum temperature for both areas increased abruptly in the late 1970s, which is also evident in the global time series and coincides with what has been described as a fundamental shift in the El Niño–Southern Oscillation phenomenon (*1*). Mean annual temperatures for the Northern and Southern hemispheres (Fig. 3) show the same abrupt increase in the late 1970s and the effect of the Mount Pinatubo eruption in 1992 (*18*). However, the temperatures for both hemispheres show a recovery to warmer temperatures, such that 1995 was the warmest year since 1950. Because maximum and minimum temperature changes are reflected in the mean, it is likely that the maximum and minimum temperature and DTR changes presented here continued to occur through 1995.

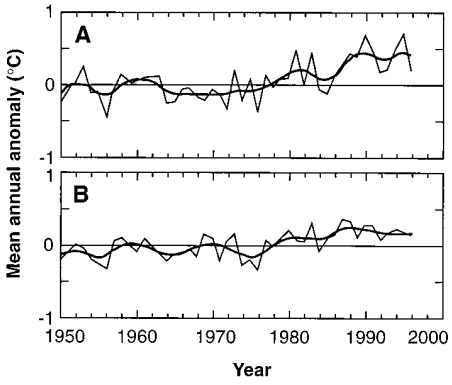

Fig. 3. Mean annual temperature anomalies (from the 1961–90 mean) for the (**A**) Northern Hemisphere and (**B**) Southern Hemisphere.

Circulation changes during the Northern Hemisphere winter were examined for a relation to the winter DTR. A westerly index (WI) was calculated from the cold ocean–warm land (COWL) pattern (*19*) and regressed against the DTR. Using yearly values, we found the correlation between the WI and DTR over the region 60°W to 90°E, 30°N to 80°N to be −0.37, significant at the 95% confidence level. There is a bipolar pattern in the relation, with positive correlations occurring over the Iberian peninsula, and negative correlations over northern Europe and into Russia. This pattern suggests that strong westerly flow is associated with increased DTR over the Iberian peninsula and decreased DTR over northern Europe and into Russia. The recent increase in WI values over the area is consistent with the observed decreasing DTR.

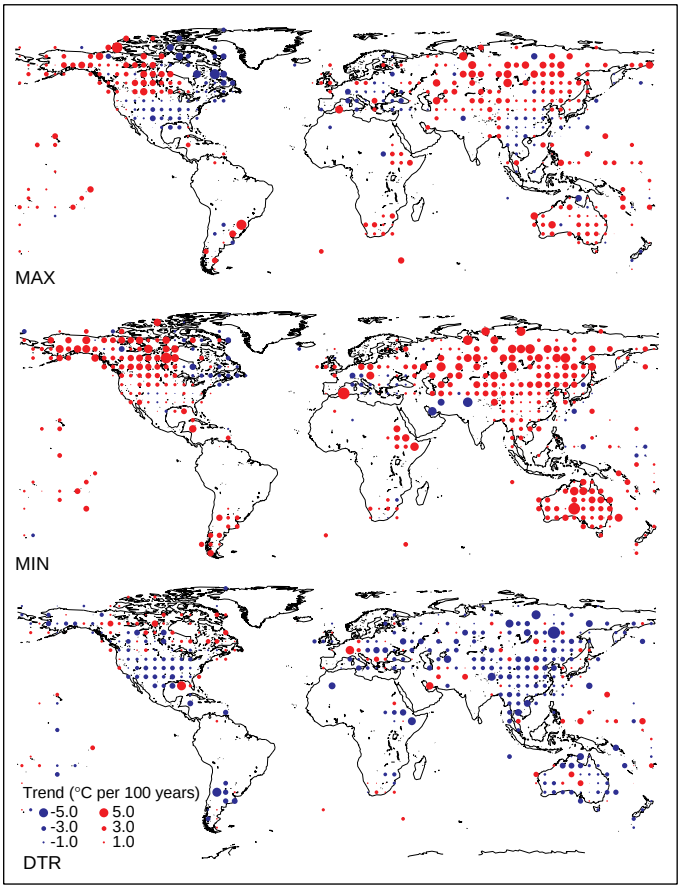

Fig. 2. Trends (in degrees Celsius per 100 years) for each 5° by 5° latitude-longitude grid box using only nonurban stations for annual maximum temperature, annual minimum temperature, and diurnal temperature range.

REFERENCES AND NOTES.

1. Intergovernmental Panel on Climate Change (IPCC), *Climate Change 1995: The Science of Climate Change*, J. T. Houghton *et al.*, Eds. (Cambridge Univ. Press, Cambridge, 1995).
2. T. R. Karl *et al.*, *Geophys. Res. Lett.* **18**, 2253 (1991).
3. T. R. Karl *et al.*, *Bull. Am. Meteorol. Soc.* **74**, 1007 (1993).
4. T. R. Karl, G. Kukla, J. Gavin, *J. Clim. Appl. Meteorol.* **23**, 1489 (1984); *ibid.* **26**, 1878 (1986); M. S. Plantico, T. R. Karl, G. Kukla, J. Gavin, *J. Geophys. Res.* **95**, 16617 (1990).
5. M. J. Salinger, *Atmos. Res.* **37**, 87 (1995).
6. R. O. Weber, P. Talkner, G. Stefanicki, *Geophys. Res. Lett.* **21**, 673 (1994).
7. K. R. Kumar, K. K. Kumar, G. B. Pant, *ibid.*, p. 677.
8. K. P. Gallo, D. R. Easterling, T. C. Peterson, *J. Clim.* **9**, 2941 (1996).
9. A. Henderson-Sellers, *GeoJournal* **27**, 255 (1992).
10. T. R. Karl, R. W. Knight, G. Kukla, J. Gavin, in *Aerosol Forcing of Climate*, R. J. Charlson and J. Heintzenberg, Eds. (Wiley, New York, 1995), pp. 363–382.
11. T. C. Peterson, V. S. Golubev, P. Ya. Groisman, *Nature* **377**, 687 (1995).
12. J. Hansen, M. Sato, R. Ruedy, *Atmos. Res.* **37**, 175 (1995); G. L. Stenchikov and A. Robock, *J. Geophys. Res.* **100**, 26211 (1995).
13. D. R. Easterling and T. C. Peterson, *Int. J. Climatol.* **15**, 369 (1995).
14. _____ and T. R. Karl, *J. Clim.* **9**, 1429 (1996).
15. This paucity of data may become less of a problem with the introduction of maximum and minimum temperatures into the CLIMAT messages transmitted by the World Meteorological Organization. However, there would still be a gap between the end of currently archived data and the end of 1994, when the new CLIMAT message format became

effective. Furthermore, some of the country data used here are continually updated and improved in an effort to provide better regional analyses (for example, Australia) [S. Torok and N. Nicholls, *Aust. Meteorol. Mag.* **45**, 251 (1996)].
16. T. C. Peterson *et al.*, in *Proceedings of the 7th Symposium on Global Change Studies* (American Meteorological Society, Boston, MA, 1996), pp. 77–78.
17. P. D. Jones *et al.*, *Nature* **347**, 169 (1990).
18. P. D. Jones, *J. Clim.* **7**, 1794 (1994).
19. J. M. Wallace, Y. Zhou, L. Bajuk, *ibid.* **9**, 249 (1996).
20. We thank P. Ya. Groisman for his insightful comments. Partial support for this work was provided by the U.S. Department of Energy.

3 March 1997; accepted 2 May 1997

Precursor-Directed Biosynthesis of Erythromycin Analogs by an Engineered Polyketide Synthase

John R. Jacobsen, C. Richard Hutchinson, David E. Cane, Chaitan Khosla*

A genetic block was introduced in the first condensation step of the polyketide biosynthetic pathway that leads to the formation of 6-deoxyerythronolide B (6-dEB), the macrocyclic precursor of erythromycin. Exogenous addition of designed synthetic molecules to small-scale cultures of this null mutant resulted in highly selective multimilligram production of unnatural polyketides, including aromatic and ring-expanded variants of 6-dEB. Unexpected incorporation patterns were observed, illustrating the catalytic versatility of modular polyketide synthases. Further processing of some of these scaffolds by postpolyketide enzymes of the erythromycin pathway resulted in the generation of novel antibacterials with in vitro potency comparable to that of their natural counterparts.

Polyketides comprise a large and diverse group of natural products, many of which possess important biological and medicinal properties (*1*), yet polyketide biosynthesis proceeds by simple, repetitive condensations of acetate or propionate monomers in a manner that closely parallels fatty acid synthesis (*2*). Structural complexity is introduced by variation in the stereochemistry and the degree of reduction after each condensation as well as by downstream enzymes that catalyze cyclizations, oxidations, alkylations, glycosylations, and other transformations. Although these compounds are an attractive target for drug discovery (*1*), the complexity of many interesting polyketides impedes the preparation of analogs. Genetic methods for manipulating polyketide synthases (PKSs) show considerable promise for the engineered biosynthesis of novel polyketide molecules (*3*) but are currently limited in the range of compounds that may be accessed. The challenges involved in total synthesis of macrolides (*4*) make this approach impractical for the preparation of derivatives. Synthetic modification of macrolides has led to the preparation of interesting compounds (*5*–*7*), but this method can also be extremely labor intensive and is limited in the range of transformations that can be selectively performed on these complex natural products. We report the development of a generally applicable, fermentation-based strategy in which chemically synthesized, cell-permeable, non-natural precursors are transformed into molecules resembling natural products by genetically engineered PKSs.

Deoxyerythronolide B synthase (DEBS) produces 6-deoxyerythronolide B (6-dEB) (**1** in Fig. 1), the parent macrolactone of the broad-spectrum antibiotic erythromycin. DEBS consists of three large polypeptides (each >300 kD), each containing ~10 distinct active sites. A one-to-one correspondence between active sites and chemical steps has been proposed (*8*, *9*), leading to a model for the synthesis of 6-dEB in which each elongation step is handled by a separate enzyme "module" [see figure 1 of (*10*)]. The modular nature of DEBS and related PKSs (*11*) suggests potential strategies for genetic manipulation to generate novel natural products. Indeed, the feasibility of generating new polyketides has been demonstrated through the use of module deletion (*12*), loss-of-function mutagenesis within reductive domains (*9*, *13*, *14*), replacement of acyltransferase domains in order to alter starter or extender unit specificity (*15*), and gain-of-function mutagenesis to introduce novel catalytic activities within modules (*16*). Importantly, many experiments show that downstream enzymes can process non-natural intermediates.

Biochemical analysis has also revealed that DEBS has considerable tolerance toward non-natural substrates. For example, primer units such as acetyl and butyryl coenzyme A (CoA) (*17*), or *N*-acetylcysteamine (NAC) thioesters of their corresponding diketides (*18*), can be incorporated in vitro into the corresponding analogs of 6-dEB. However, in the course of these studies, it became clear that, even in the absence of externally added propionyl primers, a potential non-natural substrate must compete with propionate primers derived in situ by means of enzyme-catalyzed decarboxylation of methylmalonyl extender units (*19*). This competition puts severe limits on the priming of DEBS with unnatural thioesters because, for a poorly incorporated substrate, 6-dEB would be expected to be the dominant product.

We focused on incorporating substrates in vivo as cell-permeable NAC thioesters. Although exogenously fed NAC thioesters of advanced intermediates incorporate into several natural products derived from modular PKSs, the degree of specific incorporation was low (<3%) in all cases, presumably because of competing synthesis from metabolically derived intermediates (*20*–*23*). Mutational biosynthesis (*24*) offers the advantage of eliminating such competition. For example, a randomly generated mutant strain of the avermectin producer, in which biosynthesis of branched primer units is blocked, has been used to generate avermectin derivatives of commercial utility (*21*, *25*). However, the unpredictability of random mutagenesis, coupled with the observation that incorporation efficiencies of natural and non-natural substrates by such a mutant are low (*26*), precludes the general applicability of this strategy. In contrast, the specific introduction of null mutations, facilitated by the modular nature of DEBS, provides a general method for construction of useful blocked mutants. For example, inactivation of the ketosynthase KS1 would be expected to abolish normal biosynthesis, but polyketide production might still occur if an appropriate diketide (such as **2** in Fig. 1) was supplied as an NAC thioester. This has been demonstrated in the case of an engineered bimodular derivative of DEBS (*27*). To evaluate the utility of such a mutational strategy for practical precursor-directed biosynthesis of novel, structurally complex molecules, we introduced the same KS1 null mutation in the context of the full DEBS system.

J. R. Jacobsen, Department of Chemical Engineering, Stanford University, Stanford, CA 94305–5025, USA.
C. R. Hutchinson, School of Pharmacy and Department of Bacteriology, University of Wisconsin, Madison, WI 53706, USA.
D. E. Cane, Department of Chemistry, Box H, Brown University, Providence, RI 02912, USA.
C. Khosla, Departments of Chemical Engineering, Chemistry, and Biochemistry, Stanford University, Stanford, CA 94305–5025, USA.
*To whom correspondence should be addressed.